JOURNAL OF SOLID STATE CHEMISTRY **138,** 183–192 (1998)
ARTICLE NO. SC987770

# Effect of Aliovalent Cation Doping on the Electrical Conductivity of $Na_2SO_4$: Role of Charge and Size of the Dopant

A. Singhvi, S. Gomathy, P. Gopalan,[1] and A. R. Kulkarni

*Department of Metallurgical Engineering and Materials Science, Indian Institute of Technology, Bombay 400076, India*

Received June 23, 1997; in revised form January 20, 1998; accepted February 3, 1998

**A systematic study of the effect of size of the dopant and vacancy concentration on the electrical conductivity of $Na_2SO_4$ is reported. The enhancement of conductivity, most pronounced with trivalent cation doping, and maximized for 4 m/o $Sm_2(SO_4)_3$, is more than three orders of magnitude at 200°C. The enhancement of conductivity depends on the extent of solid solubility, formation of intermediate compounds, and extent of vacancy–ion interaction. The size of the dopant influences the conductivity significantly. The effect of doping several cations simultaneously in $Na_2SO_4$ is also investigated.** 

## 1. INTRODUCTION

Between 200 and 240°C, $Na_2SO_4$ exhibits five polymorphs (1). Among these, phases V, III, and I have been well characterized. The phase transition at 241°C in $Na_2SO_4$ transforms the low-temperature orthorhombic phase III (space group, *Cmcm*) to a high-temperature hexagonal phase I ($P6_3/mmc$) (2), accompanied by increases in volume ($\sim 4\%$) and conductivity ($\sim 10$ times) (3). The conductivity of $Na_2SO_4$ decreases with increase in pressure as the free volume and space for ion movement are reduced (4). The conductivity in sodium sulfate is therefore explained on the basis of the percolation-type ion transport mechanism (5). Though the conductivity of $Na_2SO_4$(I) is relatively low [$1.8 \times 10^{-4}\,\Omega^{-1}\,cm^{-1}$ at 500°C (6)], it can be enhanced considerably by cationic substitution.

Keester *et al.* (7) reported that in $Na_2SO_4$–$MSO_4$ systems ($M$ = Ni, Mn, Cu, Co, Zn, Cd, Sr, Pb, Ba, Ca), extended solid solutions for $Na_2SO_4$(I) occur with substitutions,

$$2Na^+ \rightarrow 1M^{2+} + 1V_{Na},$$

and it is possible to incorporate trivalent ions (Fe, In, Y, Gd, La) with

$$3Na^+ \rightarrow 1M^{3+} + 2V_{Na}.$$

[1]To whom correspondence may be addressed.

Hofer *et al.* (8) studied the conductivity behavior of $Na_2SO_4$(I) solid solutions formed by the aliovalent cations $Zn^{2+}$, $Ni^{2+}$, $Sr^{2+}$, and $Y^{3+}$ and reported the presence of conductivity maxima at 7% vacancy concentration in all the solid solutions, irrespective of the size, charge, or nature of the substituting cations. Reports on the phase transition behavior and conductivity of $Na_2SO_4$–$MgSO_4$ (9) and $Na_2SO_4$–$CaSO_4$ (10) systems indicate an increase in conductivity only at high temperatures.

For $Na_2SO_4$–$Ln_2(SO_4)_3$ systems ($Ln$ = Y, La, Eu, Dy, Sm, Pr, Tm), one observes high conductivity and suppression of the phase transitions inherent to pure $Na_2SO_4$ (11–13). The conductivity enhancement in these systems is attributed to the excess of Na ion vacancies generated as a result of doping with $Ln$ ions in the $Na_2SO_4$ lattice. The conductivity behavior of $Na_2SO_4$–4 m/o $M_2(SO_4)_3$ ($M = La^{3+}$, $Sm^{3+}$, $Dy^{3+}$, $In^{3+}$) exhibits a large conductivity enhancement when the ionic radius of the dopant is close to that of host $Na^+$ (12). Studies on $Na_2SO_4$–$M_2(SO_4)_3$ ($M = Ce^{3+}$, $Gd^{3+}$, $Nd^{3+}$, $Al^{3+}$) systems also substantiate the view that the $Na^+$ conductivity depends on the dopant size (14). In these systems, a constant conductivity enhancement is observed for the guest ions ($Ce^{3+}$, $Gd^{3+}$, $Nd^{3+}$) of quasi-equal radius with $Na^+$ and a relatively lower enhancement effect for the smaller $Al^{3+}$.

The systematics of the doping in terms of solid solubility formation and vacancy concentration in $Na_2SO_4$ is not clearly understood. The objective of this work is to enhance the conductivity of $Na_2SO_4$ by doping it with cations of varying size and valency. The dopants used are sulfates of $Ba^{2+}$ (1.36 Å), $Sr^{2+}$ (1.16 Å), $La^{3+}$ (1.06 Å), $Nd^{3+}$ (1.00 Å), $Sm^{3+}$ (0.96 Å), $Y^{3+}$ (0.89 Å), $Ce^{4+}$ (0.80 Å), and $Zr^{4+}$ (0.72 Å). An attempt has been made to study the effect of size on the conductivity for a chosen vacancy concentration.

It is a well-known fact that solid electrolytes are characterized by a high degree of disorder. Can we tailor such a large disorder and would that imply a high ionic conductivity in the material? An analogous situation that existed in another area of materials, metallic glasses, can provide some insights. To synthesize metallic glasses in bulk form using



0022-4596/98 $25.00

normal cooling rates, Peker and Johnson (15) chose a composition with a wide range of metallic elements to confuse the alloy during the crystallization process, thereby successfully devising an exceptionally stable user-friendly glass. Similar confusion during the crystallization process in our systems could possibly result in a large number of free and mobile $Na^+$ that would translate into a large enhancement of the conductivity. As part of our ongoing program to engineer an electrolyte with high $Na^+$ conductivity, we have adopted the "disorder" principle by doping $Na_2SO_4$ with a large number of cations.

## 2. EXPERIMENTAL PROCEDURE

Three different compositions, namely, 2, 6, and 10 m/o dopant, of the $Na_2SO_4$–$M(SO_4)$ system were studied. Additional compositions have been investigated in the $La^{3+}$- and $Sm^{3+}$-doped systems. The dopants used were $BaSO_4$, $SrSO_4$, $La_2(SO_4)_3 \cdot xH_2O$, $Nd_2(SO_4)_3 \cdot xH_2O$, $Sm_2(SO_4)_3 \cdot xH_2O$, $Y_2(SO_4)_3 \cdot 8H_2O$, $Zr(SO_4)_2 \cdot 4H_2O$, and $Ce(SO_4)_2$.

The starting materials used were anhydrous $Na_2SO_4$ procured from Loba Chemie, Bombay, India, and dopants from Aldrich Chemicals, USA. Ultrapure $Na_2SO_4$ obtained from Aldrich Chemicals, USA, was used for measurements on the undoped samples. The powders were carefully weighed in appropriate molar quantities, ground, and then melted in porcelain crucibles. However, platinum crucibles were used to melt the undoped $Na_2SO_4$ samples. The melted samples were then quenched and powdered. For conductivity measurements, the powders were pressed into pellets (5 tons/cm$^2$). All the pellets were 2–4 mm thick and 12 mm in diameter. Gold was sputtered on the two flat surfaces of the pellet to ensure good electrical contact with the Pt electrodes of the sample holder.

The impedance was measured in the cooling cycle, at frequencies ranging from 1 Hz to 32 MHz, using a Solartron Impedance Analyzer, Model Schlumberger SI1260. The DSC measurements were made with a DSC V2.2A DuPont 9900 calorimeter. XRD patterns were recorded using Cu$K\alpha$ radiation with the help of a PW1820 Philips diffractometer.

## 3. RESULTS AND DISCUSSION

### XRD

The results of our XRD analysis are tabulated in Table 1. A typical diffractogram with all indexed peaks is shown in Fig. 1. For all the 2 m/o binary compositions, $Na_2SO_4$(V) is the majority phase (Table 1). However, with $La^{3+}$, $Y^{3+}$, $Ce^{4+}$, and $Zr^{4+}$, partial stabilization of the metastable phase III and the high-temperature phase I of $Na_2SO_4$ is also observed. With $La^{3+}$, $Y^{3+}$, $Ce^{4+}$, and $Zr^{4+}$ as dopants, a few lines in the diffractogram cannot be mapped with any known phases. Of these, the unmapped lines are reasonably strong only in the $Na_2SO_4$–$Y_2(SO_4)_3$ system.

**TABLE 1**
**Phases Observed in XRD of Some $Na_2SO_4$-Based Systems**

| | Concentration of dopant in $Na_2SO_4$ | | |
|---|---|---|---|
| Dopants | 2% | 6% | 10% |
| $BaSO_4$ | $Na_2SO_4$(V) | $Na_2SO_4$(V) | $Na_2SO_4$(V) |
| $SrSO_4$ | $Na_2SO_4$(V) | $Na_2SO_4$(V) | $Na_2SO_4$(V) |
| | | $Na_2SO_4$(III) | $Na_2SO_4$(III) |
| $La_2(SO_4)_3$ | $Na_2SO_4$(V) | $Na_2SO_4$(V) | $Na_2SO_4$(V) |
| | $Na_2SO_4$(III) | $Na_2SO_4$(III) | $Na_2SO_4$(III) |
| | $Na_2SO_4$(I) | $Na_2SO_4$(I) | $Na_2SO_4$(I) |
| | | $NaLa(SO_4)_2$ | $NaLa(SO_4)_2$ |
| $Nd_2(SO_4)_3$ | $Na_2SO_4$(V) | $Na_2SO_4$(V) | $Na_2SO_4$(V) |
| | | $Na_2SO_4$(III) | $Na_2SO_4$(III) |
| | | $Na_2SO_4$(I) | $Na_2SO_4$(I) |
| | | $Nd_2(SO_4)_3$ | $Nd_2(SO_4)_3$ |
| | | $NaNd(SO_4)_2$ | $NaNd(SO_4)_2$ |
| $Sm_2(SO_4)_3$ | $Na_2SO_4$(V) | $Na_2SO_4$(V) | $Na_2SO_4$(V) |
| | | $Na_2SO_4$(III) | $Na_2SO_4$(III) |
| | | $Na_2SO_4$(I) | $Na_2SO_4$(I) |
| | | | $NaSm(SO_4)_2$ |
| | | | $Sm_2(SO_4)_3$ |
| $Y_2(SO_4)_3$ | $Na_2SO_4$(V) | $Na_2SO_4$(V) | $Na_2SO_4$(V) |
| | $Na_2SO_4$(III) | $Na_2SO_4$(III) | $Na_2SO_4$(III) |
| | | $Na_2SO_4$(I) | $Na_2SO_4$(I) |
| | | | $Y_2(SO_4)_3$ |
| $Ce(SO_4)_2$ | $Na_2SO_4$(V) | $Na_2SO_4$(V) | $Na_2SO_4$(V) |
| | $Na_2SO_4$(III) | $Na_2SO_4$(III) | $Na_2SO_4$(III) |
| | | $Na_2SO_4$(I) | $Na_2SO_4$(I) |
| | | $NaCe(SO_4)_2$ | $NaCe(SO_4)_2$ |
| $Zr(SO_4)_2$ | $Na_2SO_4$(V) | $Na_2SO_4$(III) | $Na_2SO_4$(III) |
| | $Na_2SO_4$(III) | $Na_2SO_4$(I) | $Na_2SO_4$(I) |
| | $Na_2SO_4$(I) | | |

As the dopant concentration is increased to 6 m/o in the binary, except for the $Zr^{4+}$-doped sample, we observe that $Na_2SO_4$(V) and $Na_2SO_4$(III) are the predominant phases. In addition, all cations with the exception of $Ba^{2+}$ and $Sr^{2+}$ stabilize phase I partially. Interestingly, at room temperature, intermediate compounds such as $NaLa(SO_4)_2$, $NaNd(SO_4)_2$, and $NaCe(SO_4)_2$ are also observed, signaling a solubility limit for these cations.

For 10 m/o of the dopant in the binary, phases V, III, and I of $Na_2SO_4$ are observed at room temperature except for the $Ba^{2+}$- and $Sr^{2+}$-doped samples, which do not stabilize phase I. In addition to $NaLa(SO_4)_2$, $NaNd(SO_4)_2$, and $NaCe(SO_4)_2$, $NaSm(SO_4)_2$ is also observed. For $Y^{3+}$ and $Sm^{3+}$ compositions, peaks corresponding to the starting materials, namely, $Sm_2(SO_4)_3$ and $Y_2(SO_4)_3$, are also observed in the diffractogram.

### DSC/DTA

For the 2 m/o composition of most systems studied in this work, the peak observed around 240°C, shown in Figs. 2

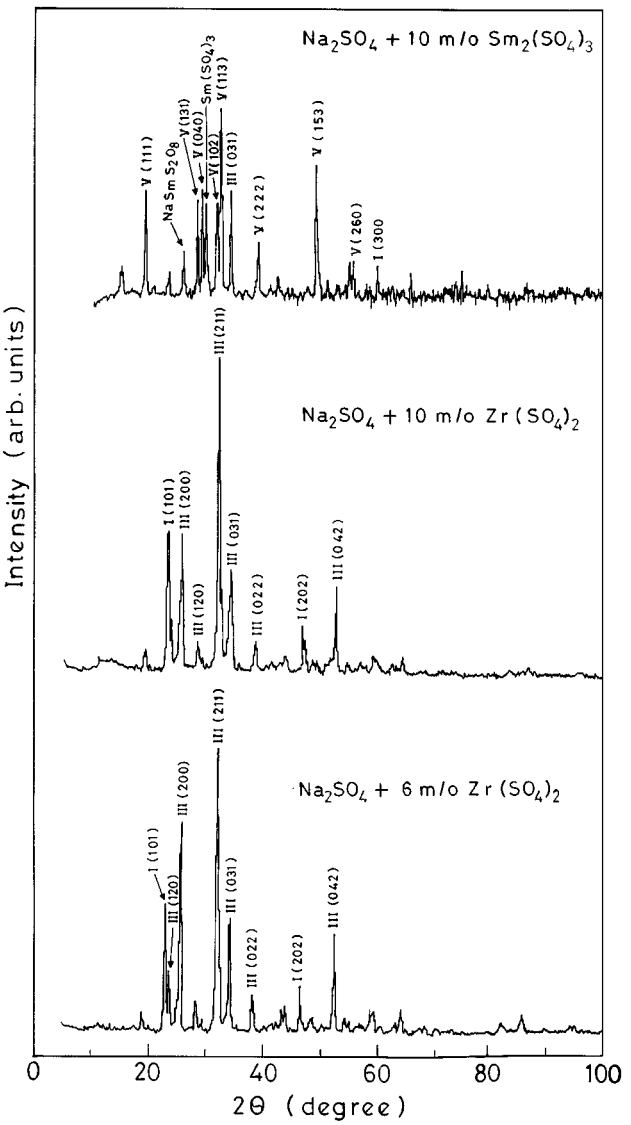


**FIG. 1.** XRD pattern for doped $Na_2SO_4$-based system.

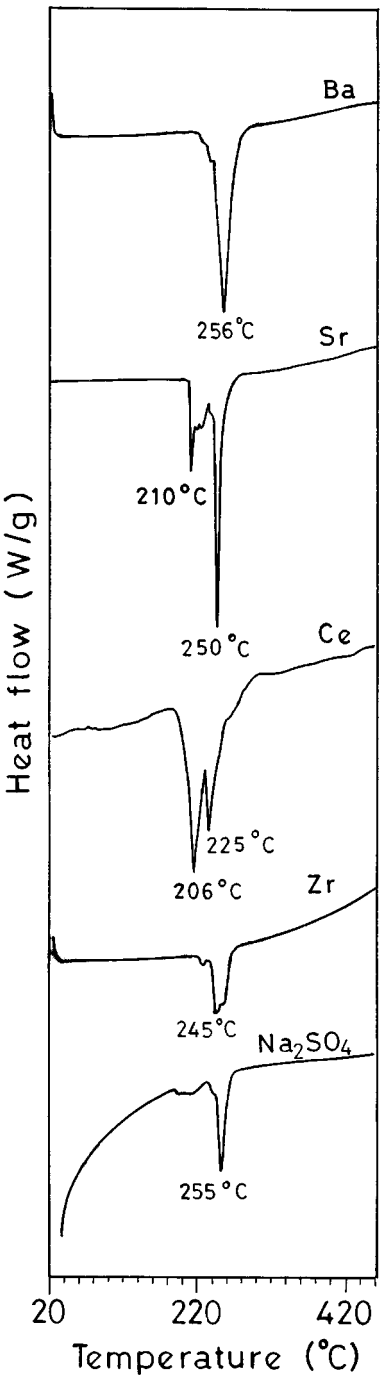


**FIG. 2.** DSC traces of $Na_2SO_4$ + 2 m/o $MeSO_4$ ($Me$ = Ba, Sr, Ce, Zr).

and 3 and tabulated in Table 2, appears associated with the V → I transition in $Na_2SO_4$. In the case of the 2 m/o composition of $Y^{3+}$ and $Ce^{4+}$, a peak around 200°C is associated with the V → I transition in $Na_2SO_4$. This is substantiated by a discontinuous change in the conductivity of these samples at around 200°C (Figs. 7, 8). For $Zr^{4+}$, the peak at 245°C does not correspond to any phase transition known in $Na_2SO_4$. The $\sigma(T)$ plot in Fig. 6 (discussed later) exhibits a V → I transition at about 180°C. The reduced peak size for the $Zr^{4+}$ sample suggests partial stabilization of $Na_2SO_4$(I) and is supported by the presence of peaks corresponding to $Na_2SO_4$(I) in the room temperature XRD. The peaks at 255 and 275°C in the composition containing 2 m/o $La^{3+}$ cannot be mapped to V → III and III → I transitions as our $\sigma(T)$ plots in Fig. 11 (discussed later) clearly indicate that phase I is stabilized at 90°C. We also observe thermal peaks at temperatures between 275 and 290°C for the $Sm^{3+}$, $Y^{3+}$, and $Nd^{3+}$-doped compositions, suggesting the formation of some intermediate compounds, in agreement with reported data (8, 16, 17).

For the 6 m/o dopant compositions, the sharp endotherm observed around 245°C (Table 2) for the $Sr^{2+}$-containing

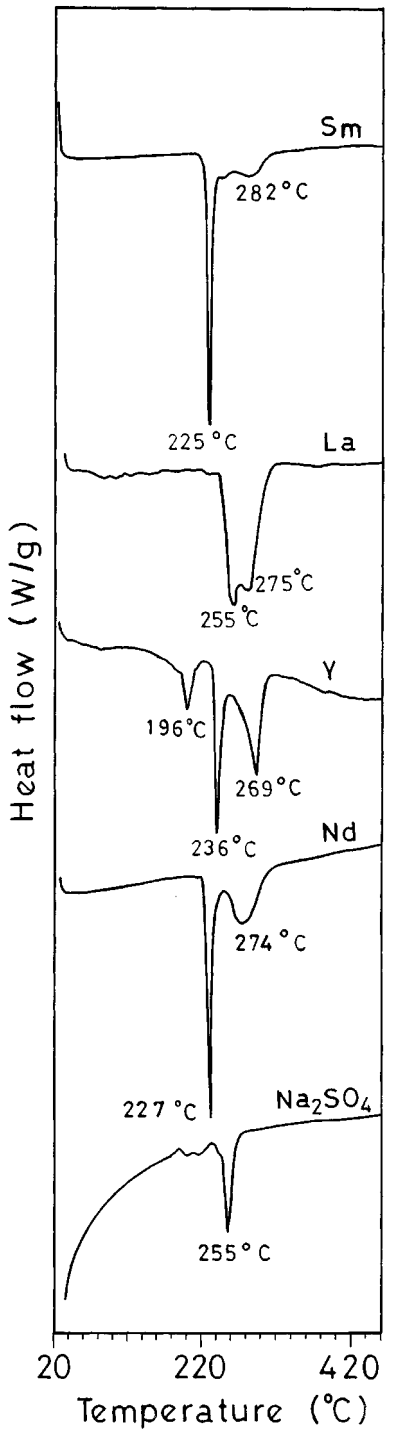


**FIG. 3.** DSC traces of $Na_2SO_4$ + 2 m/o $M_2(SO_4)_3$ ($M$ = La, Nd, Sm, Y).

**TABLE 2**
**Peaks (°C) Observed in DTA/DSC for Some $Na_2SO_4$-Based Systems**

| | Concentration of dopant in $Na_2SO_4$ | | |
|---|---|---|---|
| Dopants | 2% | 6% | 10% |
| $BaSO_4$ | 256 (V → I) | 200 (V → I), 252 | 206 (V → III), 254 (III → I) |
| $SrSO_4$ | 210 (V → III), 246 (III → I) | 235 (V → III), 245 (III → I) | 235 (V → III), 262 (III → I) |
| $La_2(SO_4)_3$ | 255, 275 | 260, 310, 336 | 267, 322, 367 |
| $Nd_2(SO_4)_3$ | 227 (V → I), 274 | 234, 283, 307 | 106, 239, 274, 328, 414 |
| $Sm_2(SO_4)_3$ | 225 (V → I) | 230 (V → I), 309 | 106, 235, 327, 394, 553, 641 |
| $Y_2(SO_4)_3$ | 196 (V → I), 236, 289 | 179, 294, 351 | 171 (V → III), 253 (III → I), 489, 666 |
| $Ce(SO_4)_2$ | 206 (V → I), 225 | 230, 297 | 224, 279 |
| $Zr(SO_4)_2$ | 245 | 196 (V → III) | — |

composition corresponds to the III → I transition in $Na_2SO_4$. The absence of any significant peak for the $Zr^{4+}$ composition points to a trend toward partial to complete stabilization of $Na_2SO_4$(I). However, our conductivity results in Fig. 6 clearly point to a well defined V → I transition. There is considerable work in the literature (18, 19) with other dopants that is consistent with these observations. As before, the endotherm observed at higher temperatures, between 240 and 350°C, for $La^{3+}$, $Sm^{3+}$, $Y^{3+}$, $Ce^{4+}$, and $Nd^{3+}$ suggests the formation of intermediate compounds.

For the 10 m/o $Ba^{2+}$ and the $Sr^{2+}$ compositions, the endotherms at around 206 and 235°C, respectively, confirm that $Na_2SO_4$(V) is the stable phase. This is supported by our XRD data for these two cations. At the 10 m/o level of doping, the large number of endotherms and some exotherms observed for the $Sm^{3+}$- and $Nd^{3+}$-containing compositions at higher temperatures (Table 2) add to the complexity of our analysis. The absence of any phase diagram for the $Na_2SO_4$–$Sm_2(SO_4)_3$ and $Na_2SO_4$–$Nd_2(SO_4)_3$ binary systems makes any interpretation awkward. It appears that the number of peaks increase due to compound formation as the solubility limit is exceeded. Consistent with earlier works (12, 17), the endotherms at higher temperatures ( > 275°C) for the $Ce^{4+}$, $La^{3+}$, and $Y^{3+}$ compositions appear to correspond to the formation of intermediate compounds. For the 10 m/o $Zr^{4+}$ composition, we do not see any significant peak in the DTA/DSC experiments.

### Ionic Conductivity

#### *Conductivity versus Temperature*

Plots of $\log \sigma$ versus $10^3/T$ are shown in Figs. 4 through 11. In Fig. 4, for $Ba^{2+}$ (1.36 Å), at any given temperature, above the III → I transition temperature, the conductivity increases with increasing dopant concentration, in

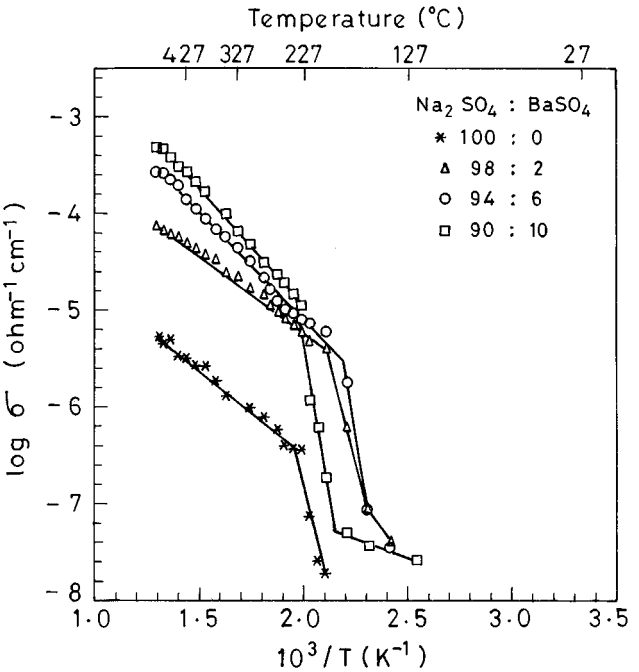


**FIG. 4.** Log $\sigma$ versus $10^3/T$ for three different compositions of $Na_2SO_4$–$BaSO_4$ system.

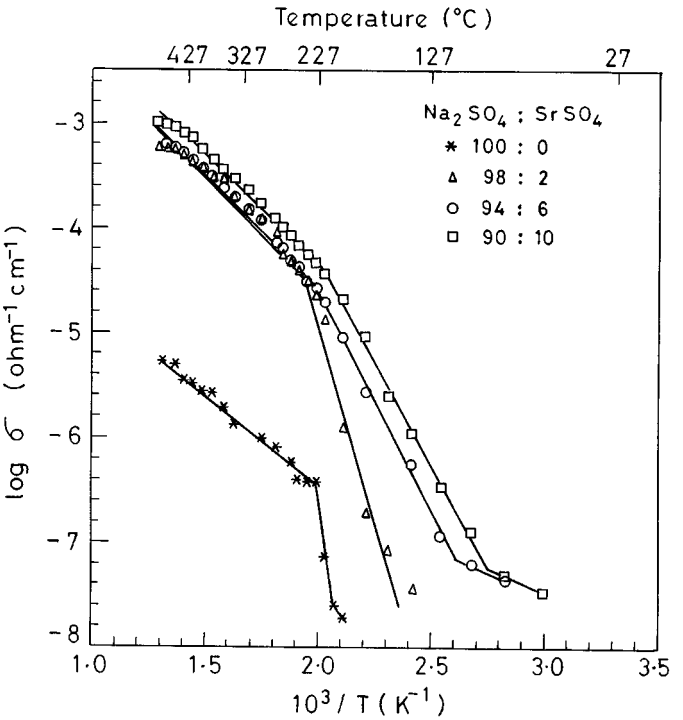


**FIG. 5.** Log $\sigma$ versus $10^3/T$ for three different compositions of $Na_2SO_4$–$SrSO_4$ system.

agreement with the limit of solid solubility in the $Na_2SO_4$–$BaSO_4$ binary being 21 m/o $BaSO_4$ (18).

Above the III → I transition temperature, the difference in conductivity between the three compositions of $Ba^{2+}$ is significant only at higher temperatures. This can be argued on the lines that at about $\sim 255°C$ ($T_c$), the vacancy–impurity clusters impede the motion of vacancies for the higher dopant concentrations. However, at higher temperatures, the thermal energy breaks up these clusters, rendering more vacancies mobile.

Similar features are observed in the $Na_2SO_4$–$SrSO_4$ binary (in Fig. 5) where the limit of solid solubility is known to be 17 m/o $SrSO_4$ (19). The difference in conductivity is minimal for the three compositions of $Sr^{2+}$ (1.16 Å), attributed to the possibility of a stronger binding between the impurities and vacancies. Our conductivity results for 2 m/o $Sr^{2+}$ are in agreement with the reported values in Hofer *et al.* (8).

For the smallest dopant, $Zr^{4+}$ (0.72 Å), we find that the conductivity is highest for the 6 m/o $Zr(SO_4)_2$ composition (Fig. 6). Each $Zr^{4+}$ generates three $Na^+$ vacancies and hence, unlike $Ba^{2+}$ and $Sr^{2+}$, which generate only one vacancy, clearly a lower doping level of $Zr(SO_4)_2$ should yield the highest conductivity. This is indeed the case, as the conductivity exhibits a maximum for 6 m/o $Zr(SO_4)_2$. At 10 m/o $Zr(SO_4)_2$, the impurity–vacancy clusters are responsible for the lower conductivity, a feature that has been observed for compositions containing large amounts of dopant in most systems studied in this work.

Similar to the behavior observed for $Zr^{4+}$, in the $Ce^{4+}$ (0.80 Å) system, the 6 m/o $Ce(SO_4)_2$ composition in Fig. 7 exhibits the highest conductivity. However, a single slope

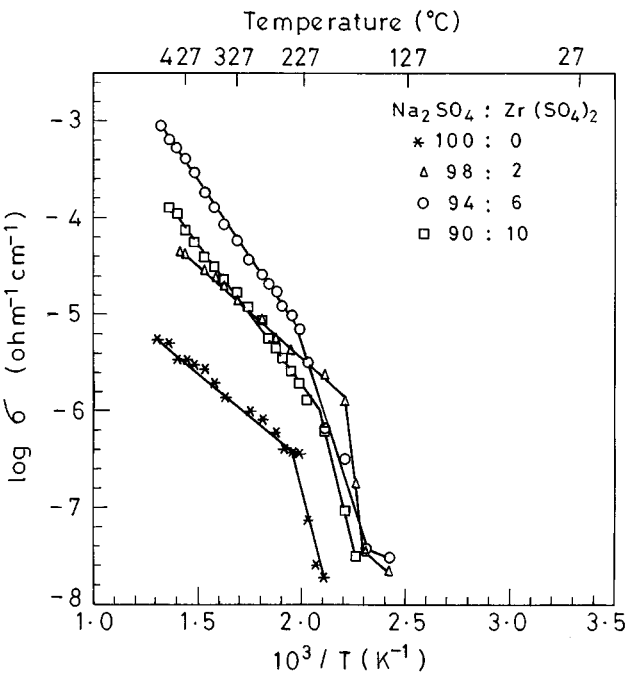


**FIG. 6.** Log $\sigma$ versus $10^3/T$ for three different compositions of $Na_2SO_4$–$Zr(SO_4)_2$ system.

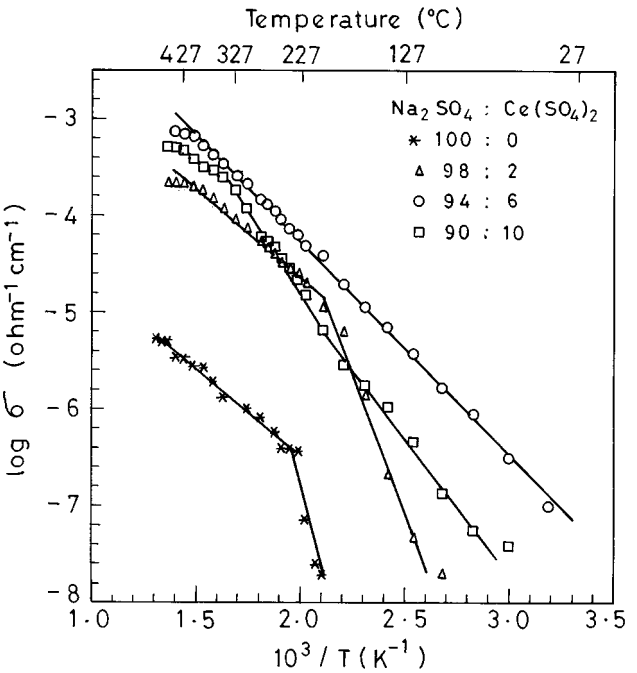


**FIG. 7.** Log $\sigma$ versus $10^3/T$ for three different compositions of $Na_2SO_4$–$Ce(SO_4)_2$ system.

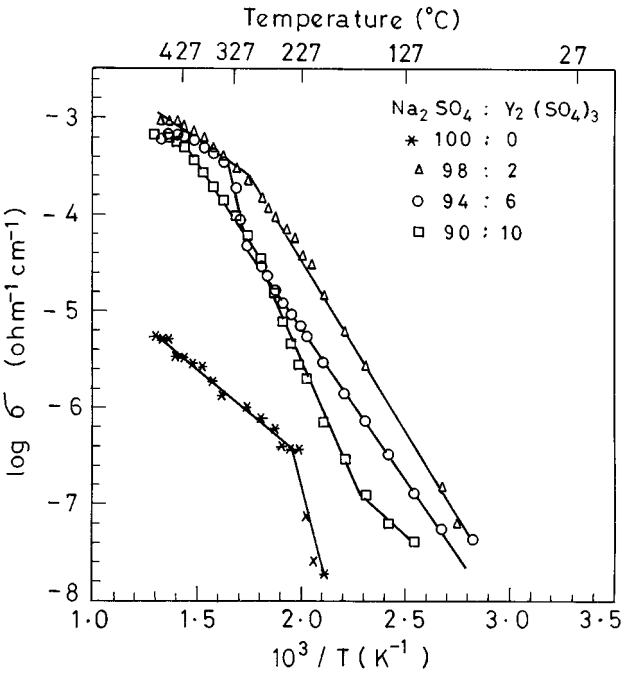


**FIG. 8.** Log $\sigma$ versus $10^3/T$ for three different compositions of $Na_2SO_4$–$Y_2(SO_4)_3$ system.

for this composition between 300 and 700 K indicates that $Na_2SO_4$(I) has been stabilized at room temperature, ruling out the 230°C peak in DTA as a transition associated with $Na_2SO_4$. The higher conductivity of 10 m/o $Ce(SO_4)_2$ relative to that of 2 m/o $Ce(SO_4)_2$ at temperatures above 250°C has been attributed to the possibility of increased solubility of $Ce^{4+}$ in $Na_2SO_4$. Furthermore, while 10 m/o $Ce(SO_4)_2$ exhibits the high-conducting phase I even at room temperature, the dominant phase at lower temperatures in the 2 m/o $Ce(SO_4)_2$ sample is the relatively low-conducting phase III.

For the $Y^{3+}$ (0.89 Å) system, the conductivity results displayed in Fig. 8 reveal that in the low-temperature range, the 2 m/o $Y_2(SO_4)_3$ composition exhibits the largest conductivity. Though the room-temperature XRD reveals only $Na_2SO_4$(V) for the 2 m/o $Y_2(SO_4)_3$ composition, we are unable to detect the V → I transition in our conductivity studies on cooling to 90°C. At higher temperatures, the conductivities of 6 and 10 m/o $Y_2(SO_4)_3$ become comparable to that of 2 m/o $Y_2(SO_4)_3$. This can be attributed to an increase in the number of mobile vacancies that contribute to conductivity. The transitions in conductivity for the 6 m/o composition at ~300°C and for the 10 m/o composition at about ~460°C compare well with the peaks in the thermogram for these compositions (Table 2). However, in the absence of the $Na_2SO_4$–$Y_2(SO_4)_3$ phase diagram, little can be said about these transitions. Though our values of conductivity are almost an order of magnitude lower to those reported for this system at 400°C (17), they are in agreement with the data reported by Hofer *et al.* at 350°C (8).

A large enhancement of conductivity has been observed for the $Na_2SO_4$–$Sm_2(SO_4)_3$ binary. Our results for the 2 m/o $Sm^{3+}$ (0.96 Å) composition are in agreement with the reported values (11). The conductivity shows a maximum with 4 m/o $Sm_2(SO_4)_3$, also in agreement with reported data (12). While the DSC scans show transitions for all the compositions, the conductivity-versus-temperature plots in Fig. 9 do not show any abrupt changes in $\sigma(T)$ anywhere below 250°C. The 6 m/o and 10 m/o $Sm^{3+}$-doped compositions show behavior almost identical to that of the $Y^{3+}$-doped system. The larger conductivity in this system for the 10 m/o composition appears to be a consequence of the known insulating characteristics of $Sm_2(SO_4)_3$ (20).

For the $Na_2SO_4$–$Nd_2(SO_4)_3$ system, as with $Y^{3+}$, the 2 m/o $Nd^{3+}$ (1.00 Å) composition exhibits the highest conductivity at any temperature. Our plot in Fig. 10 for 2 m/o $Nd_2(SO_4)_3$ shows a change in slope at about 260°C, which can be correlated with a thermal event observed in DTA at 274°C (Table 2). However, at this level of doping, very little information is available from XRD as we are below the detection threshold, and the absence of a phase diagram for this binary makes it difficult to speculate on the nature of the transition. A similar change in slope is encountered for the 6 m/o composition at a higher temperature (~370°C). For the 10 m/o composition, two such changes in slope occur, and can be related to the DTA peaks at 274, 328, and

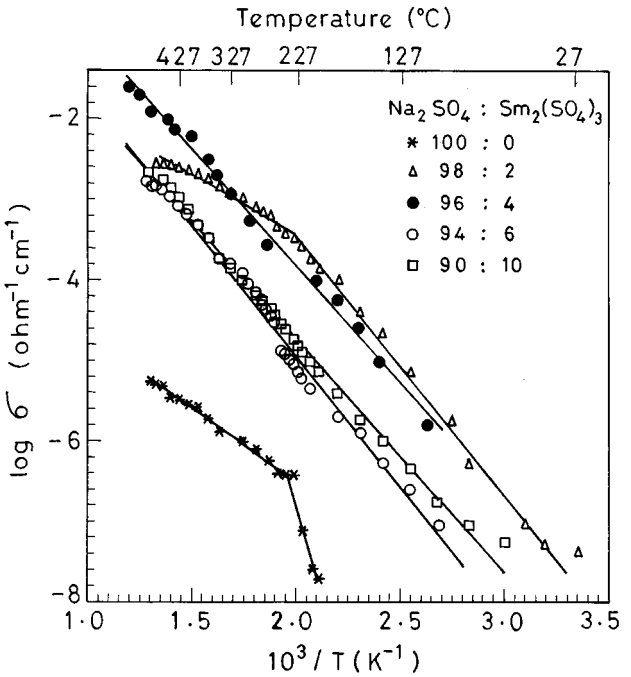


**FIG. 9.** Log $\sigma$ versus $10^3/T$ for three different compositions of $Na_2SO_4$–$Sm_2(SO_4)_3$ system.

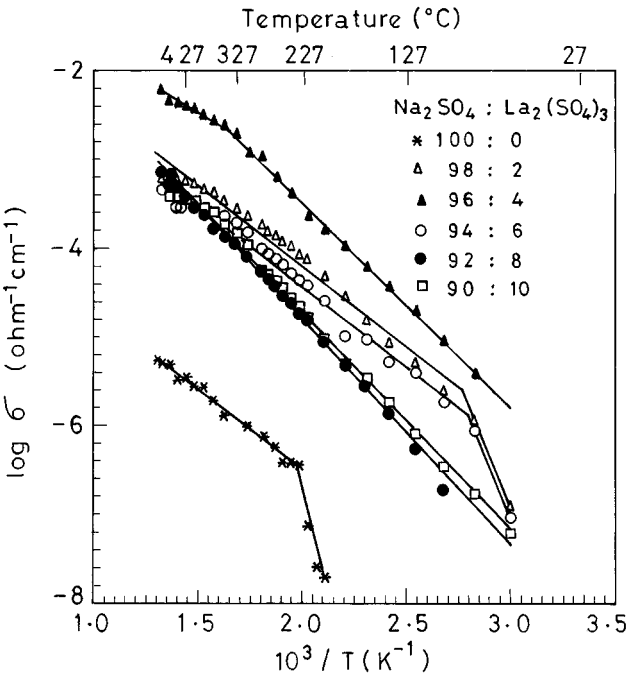


**FIG. 11.** Log $\sigma$ versus $10^3/T$ plots for three different compositions of $Na_2SO_4$–$La_2(SO_4)_3$ system.

414°C. The large number of phases encountered in XRD for the 6 and 10 m/o compositions suggests that moving across a phase boundary leads to the changes in slope observed in the conductivity. Our conductivity values for the 6 m/o composition are an order of magnitude lower than those reported by Secco (14).

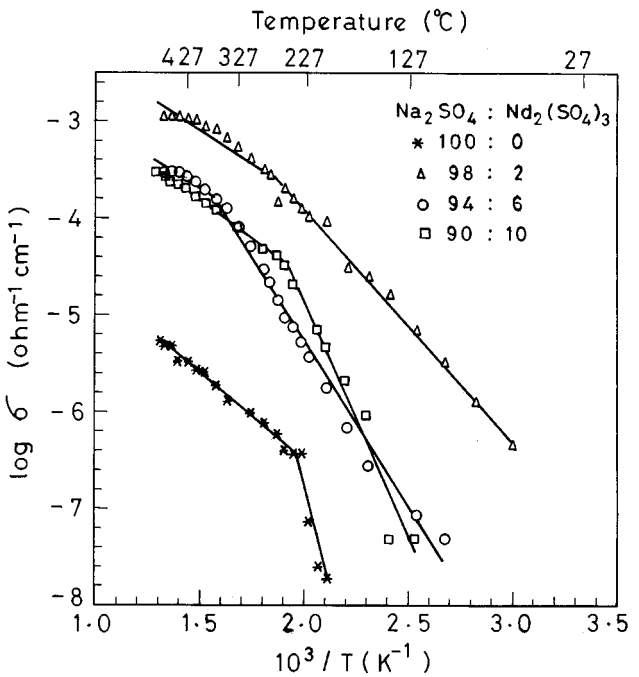


**FIG. 10.** Log $\sigma$ versus $10^3/T$ plots for three different compositions of $Na_2SO_4$–$Nd_2(SO_4)_3$ system.

The $Na_2SO_4$–$La_2(SO_4)_3$ system has been studied by more than one group (12, 17). Our plots in Fig. 11 show that the 4 m/o $La_2(SO_4)_3$ composition has the highest conductivity at any given temperature, in agreement with reported data (12). Our results are in agreement with the reported systematics, namely, that the conductivity of 2 and 6 m/o $La^{3+}$ (1.06 Å)-doped compositions are almost the same. However, the conductivity values for 2 and 6 m/o $La_2(SO_4)_3$ are somewhat lower than those reported in earlier studies (12, 17). The V → I transition for the 2 and 6 m/o compositions has been lowered to show complete stabilization at 90°C.

The lower conductivity of the 6 and 10 m/o compositions relative to that of 4 m/o composition in $Sm_2(SO_4)_3$, $Nd_2(SO_4)_3$, and $La_2(SO_4)_3$ is attributed to impurity–vacancy clusters and also to the existence of large number of phases observed in room-temperature XRD (Table 1).

Lastly, the temperature dependence of conductivity for a composition containing six dopants (90 m/o $Na_2SO_4$, 4 m/o $La_2(SO_4)_3$, 0.5 m/o $Sm_2(SO_4)_3$, 0.5 m/o $Dy_2(SO_4)_3$, 2 m/o $MgSO_4$, 2 m/o $ZnSO_4$, 1 m/o $MnSO_4$) is shown in Fig. 12. It is clearly seen that the conductivity of this composition is higher than the conductivity of 4 m/o $La_2(SO_4)_3$ only at temperatures higher than 300°C. This can be attributed to the increased solubility of all the cations in phase I and the consequent enhancement of the number of mobile

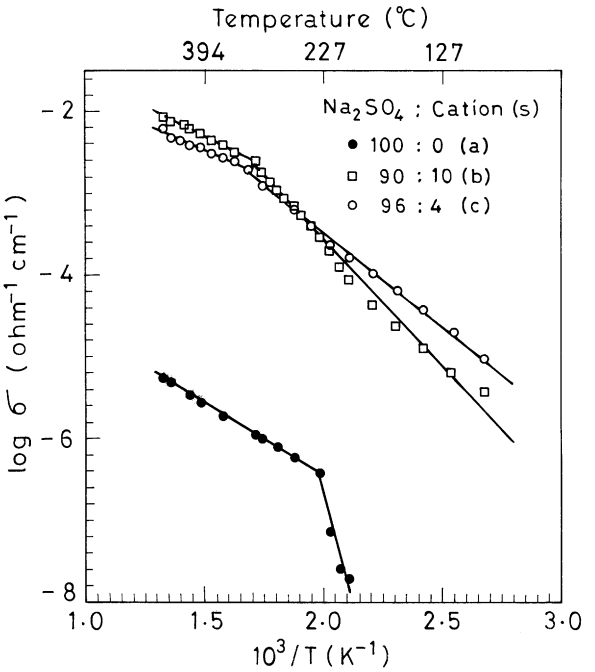


**FIG. 12.** Log $\sigma$ versus $10^3/T$ of $Na_2SO_4$ doped with several cations. (a) Pure $Na_2SO_4$. (b) 90 m/o $Na_2SO_4$ + 4 m/o $La_2(SO_4)_3$ + 0.5 m/o $Sm_2(SO_4)_3$ + 0.5 m/o $Dy_2(SO_4)_3$ + 2 m/o $MgSO_4$ + 2 m/o $ZnSO_4$ + 1 m/o $MnSO_4$. (c) 96 m/o $Na_2SO_4$ + 4 m/o $La_2(SO_4)_3$.

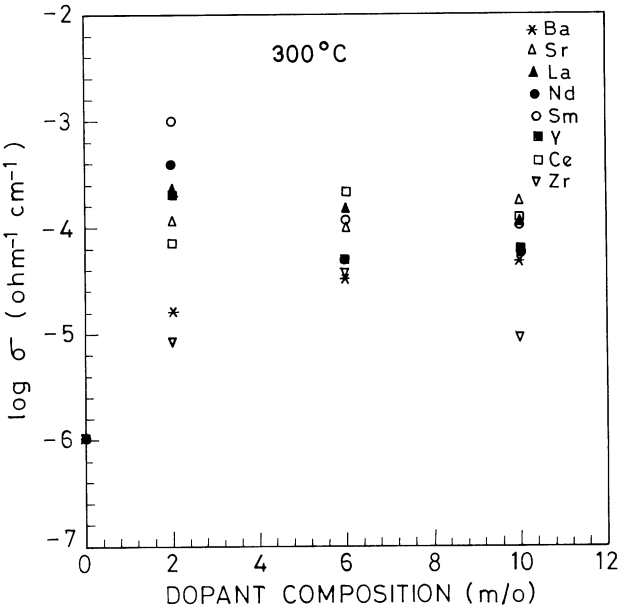


**FIG. 13.** Log $\sigma$ versus composition at 300°C.

vacancies. Thus, the *disorder principle* does not seem to result in any spectacular enhancement relative to the various binary systems we have studied.

### *Conductivity versus Composition*

The conductivity-versus-composition curves at 300°C for all the dopants are plotted in Fig. 13. At 2 m/o dopant concentration, the tetravalent ion-doped systems have lower conductivity than the di- and trivalent ion-doped systems. At this level of doping, all the vacancies generated are mobile. It is therefore evident that factors other than "wrong charge" (or vacancy concentration) contribute to the conduction process in these systems.

For $Ba^{2+}$ and $Sr^{2+}$ at 300°C (Fig. 13), conductivity increases linearly with dopant concentration, suggesting that all extrinsic vacancies are mobile. These results are consistent with the extended solid-solubility limit for these cations (21 m/o for $Ba^{2+}$ and 17 m/o for $Sr^{2+}$) in $Na_2SO_4$(I).

For $La^{3+}$ and $Sm^{3+}$, conductivity peaks for the 4 m/o composition at 300°C, in agreement with previous studies (11, 17). For these compositions, the conductivity is more than thousand times higher than that of pure $Na_2SO_4$ at around 300°C. Conductivity decreases with further increase in $M_2(SO_4)_3$ concentration because of the formation of impurity–vacancy clusters.

For the tetravalent $Zr^{4+}$ and $Ce^{4+}$, conductivity shows a maximum at 6 m/o dopant concentration. At this level of doping, assuming complete solubility, more cation vacancies are created relative to the situation when 2 or 4 m/o of the trivalent dopants is used. Thus, a different vacancy concentration gives rise to a conductivity maximum for $Zr^{4+}$ and $Ce^{4+}$. The simple model of cation vacancies proposed by Hofer *et al.* (8), where conductivity peaks for a given vacancy concentration (7%) regardless of the charge, size, or type of dopant, is therefore unable to explain the observed results. In this regard, our results contradict the claim of Hofer *et al.* (8) that the type of substituting cation does not matter. The conductivity-versus-composition plot at 400°C mimics the behavior observed at 300°C.

### *Conductivity versus Size*

Our conductivity data clearly suggest that the enhancement is different for the same concentration of different dopants. In view of the two contradicting views of Hofer *et al.* (8) and Prakash and Shahi (12), we have examined the role of the dopant size on the observed conductivity enhancements. Our observations are presented in Fig. 14. The sizes of the ions have been taken from the compilation of Shannon and Prewitt (21). At 400°C, it is evident that for the 2 m/o dopant concentration, the enhancement clearly exhibits a maximum when the size of the dopant approaches that of $Na^+$. We attribute this to ease of the formation of the solid solution when the ionic radius of the dopant is close to that of $Na^+$. However, for the 6 and 10 m/o compositions, additional factors such as the formation of additional

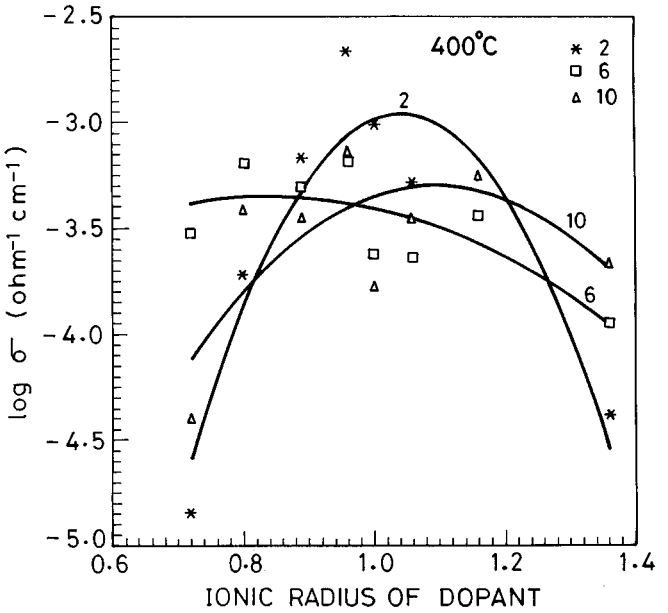


**FIG. 14.** Log $\sigma$ versus ionic radius of dopant cations at 400°C for three different composition.

phases (seen in room-temperature XRD) and impurity–vacancy clustering do not allow us to predict any trends. Thus, in addition to size, we must remember that the number of vacancies generated is different for each dopant, depending on its charge and also the extent of solid-solution formation. The effect of charge that results in generating differing numbers of vacancies for same dopant concentration can also explain the shift in peaks for the 6 and 10 m/o compositions.

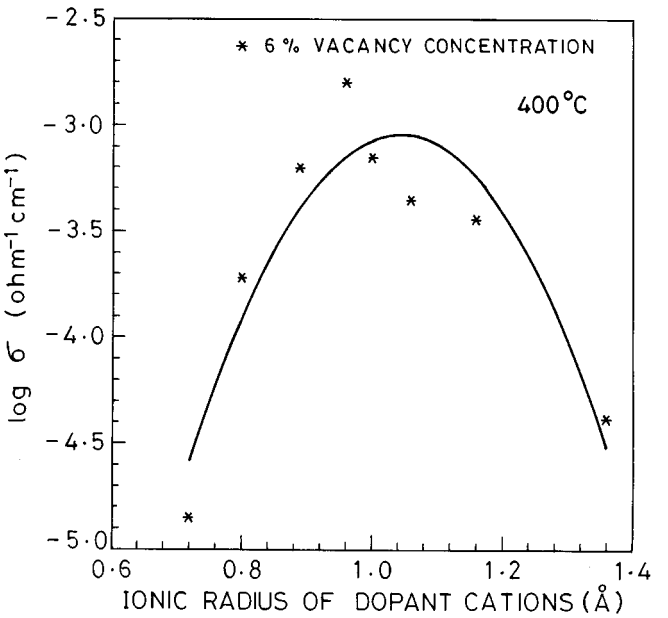


**FIG. 15.** Log $\sigma$ versus ionic radius of dopant cations at 400°C for 6% vacancy concentration.

To nullify the effect of valency of the dopant cations, we plotted the dependence of conductivity on size for a fixed vacancy (6%) concentration, thus enabling an examination of the effect of size alone. The vacancy concentrations were determined following the scheme proposed by Hofer *et al.* (8). The results of this exercise are presented in Fig. 15. The data and a fit clearly show that conductivity peaks when the dopant size is comparable to that of $Na^+$. We attribute this observation to the ease of formation of a solid solution. Furthermore, we know that lanthanum sulfate and $Na_2SO_4$(I) have a hexagonal structure, and that $r_{La^{3+}} = 1.06$ Å and $r_{Na^+} = 1.02$ Å are close; thus, solid solution formation is very easily possible. For $Sm^{3+}$, particularly for higher dopant concentrations, one must also attribute a fraction of the large conductivity to the very insulating nature of $Sm_2(SO_4)_3$ which is responsible for an interfacial contribution to $\sigma$ through the dispersoid theory (20, 22).

## 4. CONCLUSIONS

In all, eight binary systems have been studied using dopants of size varying between 0.72 and 1.36 Å. Our XRD results indicate that partial stabilization of $Na_2SO_4$(I) results with all dopants except $Ba^{2+}$ and $Sr^{2+}$. For most dopants at the 10 m/o level, we begin to observe intermediate phases.

The absence of any peak in our DSC results indicates complete stabilization of $Na_2SO_4$(I) with 10 m/o $Zr(SO_4)_2$. However, the $\sigma(T)$ results do not support this observation. In many systems studied in this work, the reduced peak as well as the area under the peak suggest partial stabilization of $Na_2SO_4$(I). In some cases, a decrease in $T_c$ for the V → I transition was also achieved (Table 2).

Our conductivity enhancements are maximum for $Sm^{3+}$ doping at 400°C. Though minimally, these results are different from known enhancements that attain a maximum in the $Na_2SO_4$–$La_2(SO_4)_3$ binary (12). The maximum value of conductivity in this work is $6.31 \times 10^{-3}$ ohm$^{-1}$ cm$^{-1}$ at 400°C for the 4 m/o $Sm_2(SO_4)_3$ composition, comparable to $7.26 \times 10^{-3}$ ohm$^{-1}$ cm$^{-1}$ at 427°C reported by Prakash and Shahi (12).

Our observations on the di-, tri-, and tetravalent dopants do not suggest the existence of a unique optimal vacancy concentration for which conductivity attains a maximum. Interestingly, a dependence of $\sigma$ on the size of dopant emerges. For a fixed vacancy concentration, the trend is very clear. Approaching the size of $Na^+$ from either side results in an enhancement of $\sigma$. We attribute this to the ease in solid solution formation.

Though the *disorder principle* does result in conductivity enhancements, the results are only marginally better at higher temperatures than for the known binary systems. We

have very few data to take a position, and a lot more work is required to draw meaningful conclusions.

Lastly, many more cations are being studied to expand on the results obtained in this work. Compositions in excess of 10 m/o divalent cations are also being investigated to ascertain the optimal dopant composition that maximizes conductivity.

## REFERENCES


1. B. N. Mehrotra, Th. Hahn, H. Arnold, and W. Eysel, *Acta Crystallogr. Sect. A* **31,** S79 (1975).
2. A. Lunden and M. A. K. L. Dissanayake, *J. Solid State Chem.* **90,** 179 (1991).
3. R. M. Murray and E. A. Secco, *Can. J. Chem.* **56,** 2616 (1978).
4. R. A. Secco and E. A. Secco, *J. Phys. Chem. Solids* **53,** 749 (1992).
5. M. D. Leblanc, U. M. Gundusharma, and E. A. Secco, *Solid State Ionics* **20,** 61 (1986).
6. K. T. Jacob and D. B. Rao, *J. Electrochem. Soc.* **126,** 1842 (1979).
7. K. L. Keester, W. Eysel, and Th. Hahn, *Acta Crystallgr. Sect. A* **31,** S79 (1975).
8. H. H. Hofer, W. Eysel, and U. von Alpen, *J. Solid State Chem.* **36,** 365 (1981); *Mater. Res. Bull.* **13,** 135 (1978).
9. P. W. S. K. Bandaranayake and B. E. Mellander, *Solid State Ionics* **40/41,** 31 (1990).
10. P. W. S. K. Bandaranayake and B. E. Mellander, *Solid State Ionics* **26,** 33 (1988).
11. K. Shahi and G. Prakash, *Solid State Ionics* **18/19,** 544 (1987).
12. G. Prakash and K. Shahi, *Solid State Ionics* **23,** 151 (1987).
13. M. Ohta and M. Sakaguchi, *J. Solid State Chem.* **91,** 57 (1991).
14. E. A. Secco, *in* "Solid State Ionics, Materials and Applications" (B. V. R. Chowdari, S. Singh, S. Chandra, and P. C. Srivastava, Eds.), p. 47, World Scientific, Singapore, 1992; E. A. Secco and M. G. Usha, *Solid State Ionics* **68,** 213 (1994).
15. A. Peker and W. I. Johnson, *Appl. Phys. Lett.* **63,** 2342 (1993).
16. N. Imanaka, S. Kuwabara, G. Y. Adachi, and J. Shiokawa, *Bull. Chem. Soc. Jpn.* **58,** 5 (1985).
17. N. Rao and J. Schoonman, *Solid State Ionics* **57,** 159 (1992).
18. Y. Saito, K. Kobayashi, and T. Maruyama, *Solid State Ionics* **3/4,** 687 (1981).
19. W. Eysel, H. H. Hofer, K. L. Keester, and Th. Hahn, *Acta Crystallogr. Sect. B* **41,** 5 (1985).
20. S. Chaklanobis, R. K. Syal, and K. Shahi, *in* "Solid State Ionics, Materials and Applications" (B. V. R. Chowdari, S. Singh, S. Chandra, and P. C. Srivastava, Eds.), p. 441, World Scientific, Singapore (1992).
21. R. D. Shannon and C. T. Prewitt, *Acta Crystallogr. Sect. B* **25,** 925 (1969).
22. A. D. Brailsford, *Solid State Ionics* **21,** 159 (1986).